

RESULTS ON DIFFRACTION ^a

K. GOULIANOS

*The Rockefeller University, 1230 York Avenue
New York, NY 10021, USA*

Results on hard diffraction from HERA and $p\bar{p}$ Colliders are reviewed with emphasis on the factorization properties of the diffractive structure function of the proton and on the structure of the pomeron.

1 Introduction

In the past few years the field of diffraction has experienced a renaissance. Experiments at $p\bar{p}$ Colliders and at HERA have been probing the diffractive structure function of the proton, shedding light at the intricate interplay between soft and hard diffraction. While a firm QCD based theoretical interpretation of the experimental results is still lacking, a rather clear phenomenological picture of the connection between soft and hard diffraction has emerged. In this picture, the (virtual) pomeron, which is presumed to be exchanged in diffractive processes, appears as a simple color-singlet construct of quarks and gluons. Its partonic structure is surprisingly hard (each parton carries a large fraction of the pomeron momentum) and, unlike that of real hadrons, persists being hard at high values of Q^2 . The wealth of the accumulated experimental data allows questions to be asked about the factorization properties of the diffractive structure function of the proton, the uniqueness of the pomeron structure, and the momentum sum rule for the pomeron. In this paper, we review the experimental results with emphasis on what is deemed to be directly relevant to answering these questions. After a brief general discussion of diffraction, we present results from the $S\bar{p}pS$ Collider, from HERA and from the Tevatron, relate the HERA and Collider results, and draw conclusions.

2 Soft and Hard Diffraction

Single diffraction (SD) dissociation accounts for approximately 10% of the total hadronic cross sections ¹. At high energies, the cross section for SD is

^aPresented at the XVIIth International Conference on Physics in Collision, Bristol, UK, 25-27 June 1997.

dominated by pomeron (\mathbb{P}) exchange. For $p\bar{p} \rightarrow pX$, it has the form

$$\frac{d^2\sigma_{SD}}{d\xi dt} = \frac{\beta_{\mathbb{P}p}^2(t)}{16\pi} \xi^{1-2\alpha(t)} \left[\beta_{\mathbb{P}p}(0) g(t) \cdot (s'/s_0)^{\alpha(0)-1} \right] \quad (1)$$

where $\alpha(t) = 1 + \epsilon + \alpha't$ is the pomeron Regge trajectory, $\beta_{\mathbb{P}p}(t)$ is the coupling of the pomeron to the proton, $g(t)$ the triple-pomeron coupling, s' the $\mathbb{P} - \bar{p}$ center of mass energy squared, $\xi \equiv x_{\mathbb{P}} = s'/s \approx M^2/s$ the fraction of the momentum of the proton carried by the pomeron, M the diffractive mass and s_0 an energy scale not specified by the theory. Experimentally, the triple-pomeron coupling was found not to depend on t ¹. A recent determination of ϵ from a global fit to $p^\pm p$, $\pi^\pm p$ and $K^\pm p$ total cross sections and ρ -values yielded² $\epsilon = 0.104 \pm 0.002$; from elastic scattering data, $\alpha' \approx 0.25 \text{ GeV}^{-2}$.

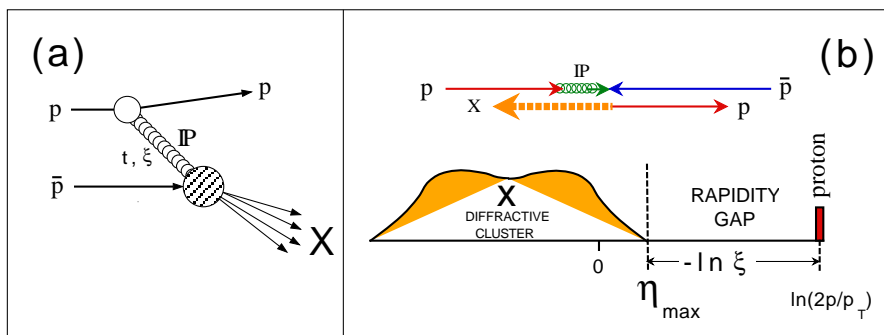


Figure 1: (a) Feynman diagram and (b) event topology for $p\bar{p}$ diffraction dissociation.

The term in brackets in (1) is identified as the $\mathbb{P} - \bar{p}$ total cross section (see Fig. 1a) and therefore the factor

$$f_{\mathbb{P}/p}(\xi, t) \equiv \frac{\beta_{\mathbb{P}p}^2(t)}{16\pi} \xi^{1-2\alpha(t)} = \frac{\beta_{\mathbb{P}p}^2(0)}{16\pi} \xi^{1-2\alpha(t)} F^2(t) = K \xi^{1-2\alpha(t)} F^2(t) \quad (2)$$

is interpreted as a ‘‘pomeron flux’’ per proton. In the Ingelman-Schlein (IS) model³ the pomeron flux is used as a luminosity factor in calculating the rates of hard processes in diffraction dissociation (hard diffraction). Such calculations are usually performed using the Monte Carlo simulation program POMPYT⁴, which combines routines that generate the pomeron ξ and t with the program PYTHIA⁵, which ‘‘performs’’ the collision.

At small t , $F^2(t) \approx e^{4.6t}$. Donnachie and Landshoff (DL) proposed a model⁶ in which $F(t)$ is identified as the isoscalar form factor measured in

electron-nucleon scattering,

$$F_1(t) = \frac{4m^2 - 2.8t}{4m^2 - t} \left[\frac{1}{1 - t/0.7} \right]^2 \quad (3)$$

where m is the mass of the proton. In the DL model, the factor K in the pomeron flux is $K_{DL} = (3\beta_{\mathbb{P}q})^2/4\pi^2$, where $\beta_{\mathbb{P}q}$ is the \mathbb{P} -quark coupling.

Figure 1b shows the event topology in pseudorapidity space for $p\bar{p} \rightarrow pX$. It is characterized by a “leading” proton at large rapidity, and a rapidity gap (absence of particles) in the region between the leading proton and the “diffractive cluster” of particles resulting from the $\mathbb{P} - \bar{p}$ collision. These characteristics are used to “tag” diffractive events.

The normalization of the pomeron flux depends on $\beta_{\mathbb{P}p}(0)$, which is determined from the experimentally measured pp total cross section, $\sigma_T^{pp} = \beta_{\mathbb{P}p}^2(0) \cdot (s/s_0)^\epsilon$. Therefore, $\beta_{\mathbb{P}p}(0)$ depends on the value of the energy scale s_0 , which, as mentioned above, is not given by the theory (s_0 is usually set to 1 GeV², the hadron mass scale, but this is only a *convention*). Thus, the normalization of the pomeron flux is unknown, and hence only predictions for *relative* hard diffraction rates are possible in the IS model.

The flux normalization uncertainty is resolved in the flux renormalization model of Goulianos⁷. The *renormalized* flux is defined as

$$f_N(\xi, t) \equiv D_N \cdot f_{\mathbb{P}/p}(\xi, t; s_0); \quad D_N = 1 / \int_{\xi_{min}}^{0.1} \int_0^\infty f_{\mathbb{P}/p}(\xi, t; s_0) d\xi dt \quad (4)$$

where $f_{\mathbb{P}/p}(\xi, t; s_0)$ is the *standard* flux and D_N is the renormalization or flux discrepancy factor⁷. The integration over ξ is carried out between the lowest kinematically allowed value, $\xi_{min} = M_0^2/s$, where $M_0^2 = 1.5$ GeV² is the effective diffractive threshold⁷, and $\xi_{max} = 0.1$, which is the “coherence limit”¹. Such a normalization, which corresponds to *at most* one pomeron per proton, leads to interpreting the pomeron flux as a probability density describing the ξ and t distributions of the exchanged pomeron.

As indicated explicitly in (4), the renormalized flux does not depend on the energy scale s_0 . Thus, using this flux, *robust* predictions for hard diffraction can be obtained not only for relative but also for absolute rates.

The renormalized pomeron flux model is supported by the s -dependence of the total and differential $pp/\bar{p}p$ SD cross sections. With the standard flux, the total and $t = 0$ differential diffractive cross sections vary as

$$\sigma_{SD}(s) \sim s^{2\epsilon} \quad \left. \frac{d^2\sigma_{SD}}{dt dM^2} \right|_{t=0} \sim \frac{s^{2\epsilon}}{(M^2)^{1+\epsilon}} \quad (5)$$

The $\sim s^{2\epsilon}$ dependence eventually leads to diffractive cross sections larger than the total and therefore to violation of unitarity. The flux renormalization

factor varies as $D_N \sim s^{-2\epsilon}$, canceling the $s^{2\epsilon}$ growth of the standard flux and preserving unitarity. Figure 2 shows that the standard flux fails to describe the data, but the renormalized flux predicts the observed s -dependence^{7,8,9}.

In terms of the rapidity gap, Δy , the pomeron flux is given by

$$\Delta y = \ln \frac{1}{\xi} \Rightarrow f_{\mathbb{P}/p}(\Delta y, t) = K \cdot e^{2(\epsilon + \alpha' t)\Delta y} \cdot F^2(t) \quad (6)$$

Since ϵ is small and $\alpha' |t| \ll \epsilon$, the flux varies slowly with Δy , approximately as $1 + 2\epsilon \Delta y$. In this “gap representation”, the renormalized flux will be referred to as the *scaled gap probability*.

In the following sections, both the standard and renormalized flux predictions for hard diffraction rates will be compared with data.

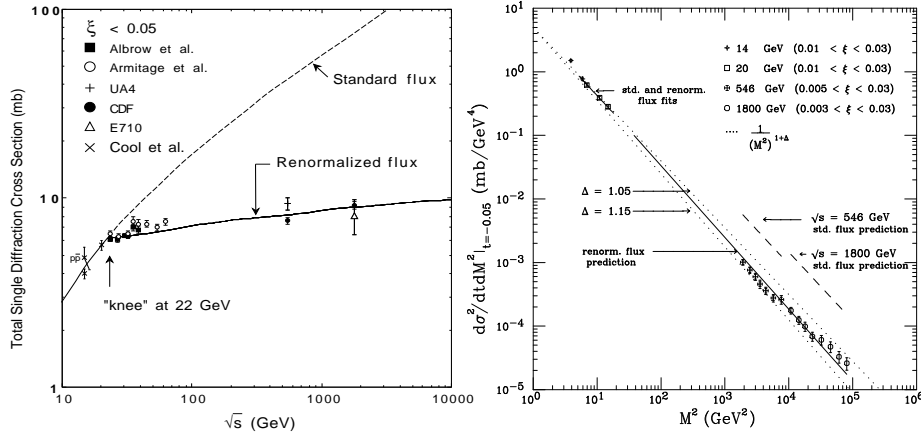


Figure 2: $p - p(\bar{p})$ diffractive cross sections: (left) $2\sigma_{SD}(s)$; (right) $d^2\sigma/dtdM^2$ at $t=-0.05$.

3 Results from the $S\bar{p}pS$ Collider

At the CERN $S\bar{p}pS$ Collider^b, the UA8 experiment pioneered hard diffraction studies by observing high- p_T jet production in the process $p + \bar{p} \rightarrow p + Jet_1 + Jet_2 + X$ at $\sqrt{s} = 630$ GeV. Events with two jets of $p_T > 8$ GeV were detected in coincidence with a high- x_F proton, whose momentum and angle were measured in a forward “roman pot” spectrometer. The event sample spanned the kinematic range $0.9 < x_p < 0.94$ and $0.9 < |t| < 2.3$ GeV². By

^bThis section is an excerpt from Ref.¹⁰

comparing the x_F distribution of the sum of the jet momenta in the pomeron-proton rest frame with Monte Carlo distributions generated with different pomeron structure functions, UA8 concluded¹¹ that the partonic structure of the pomeron is $\sim 57\%$ *hard* [$6\beta(1-\beta)$], $\sim 30\%$ *superhard* [$\delta(1-\beta)$], and $\sim 13\%$ *soft* [$6(1-\beta)^5$], where β is the fraction of the momentum of the pomeron carried by its parton constituent. However, the measured dijet production rate was found to be smaller than the rate predicted by POMPYT, using the standard flux and assuming a hard-quark(gluon) pomeron, by a (discrepancy) factor of¹² $0.46 \pm 0.08 \pm 0.24$ ($0.19 \pm 0.03 \pm 0.10$). Using the renormalized pomeron flux, the discrepancy factor becomes consistent with unity⁷.

4 Results from HERA

At HERA, where ~ 28 GeV electrons are brought into collision with ~ 800 GeV protons ($\sqrt{s} \approx 300$ GeV), diffraction has been studied both in photo-production and in high Q^2 deep inelastic scattering (DIS). The H1 and ZEUS Collaborations have measured the diffractive structure function of the proton and its internal factorization properties. Below, we review the results of these measurements and their relevance to the structure of the pomeron.

4.1 Diffractive DIS kinematics

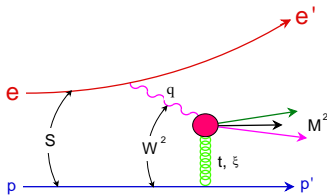


Figure 3: Schematic diagram of a diffractive DIS collision involving a virtual photon, emitted by an electron, and a virtual pomeron, emitted by a proton.

In addition to the standard DIS kinematical variables (see Fig. 3),

$$Q^2 = -q^2 \quad x_{bj} = \frac{Q^2}{2q \cdot p} \quad y = \frac{q \cdot p}{e \cdot p} \quad W^2 = (q + p)^2 \quad s = (e + p)^2 \quad (7)$$

the following variables are used to describe *diffractive* DIS:

$$\beta = \frac{Q^2}{2q \cdot (p - p')} = \frac{Q^2}{M_X^2 + Q^2 - t} \quad \xi = \frac{q \cdot (p - p')}{q \cdot p} = \frac{M_X^2 + Q^2 - t}{W^2 + Q^2 - m_p^2} \quad (8)$$

Note that $x_{bj} = \beta\xi$, so that β may be interpreted as the fraction of the momentum on the pomeron carried by the scattered parton. Of course, these kinematics are valid not only for pomeron, but for *any* exchange.

4.2 The diffractive structure function $F_2^{D(3)}$

In an analogy with the structure function $F_2(x, Q^2)$, the 4-variable diffractive structure function (DSF) of the proton is defined through the equation

$$\frac{d^4\sigma}{dQ^2 d\beta d\xi dt} = \frac{4\pi\alpha^2}{\beta Q^4} \left(2 - 2y + \frac{y^2}{2(1+R)} \right) \cdot F_2^{D(4)}(Q^2, \beta, \xi, t) \quad (9)$$

The H1 and ZEUS data presented in this paper are integrated over t within the region $|t_{min}| < |t| < 1 \text{ GeV}^2$. The t -integrated DSF, $F_2^{D(3)}$, was determined from the data by assuming $R = 0$ in (9). Thus, the measured $F_2^{D(3)}$ is defined by

$$\frac{d^3\sigma}{dQ^2 d\beta d\xi} \Big|_{|t|<1} \equiv \frac{4\pi\alpha^2}{\beta Q^4} \left(2 - 2y + \frac{y^2}{2} \right) \cdot F_2^{D(3)}(Q^2, \beta, \xi) \quad (10)$$

4.3 Gap factorization of $F_2^{D(3)}$

From an analysis of their 1993 data, both the H1¹³ and ZEUS¹⁴ Collaborations found that $F_2^{D(3)}$ has the form

$$F_2^{D(3)}(Q^2, \beta, \xi) = \frac{1}{\xi^n} \cdot A(Q^2, \beta) \quad (11)$$

The kinematic range of the measurements was

$$\begin{array}{lll} \text{H1} & 3.0 \times 10^{-4} < \xi < 0.05 & 8.5 < Q^2 < 50 \text{ GeV}^2 \\ \text{ZEUS} & 6.3 \times 10^{-4} < \xi < 0.01 & 10 < Q^2 < 63 \text{ GeV}^2 \end{array}$$

The factorized form (11) is what is expected from the IS model³, in which the $F_2^{D(4)}$ is given by the pomeron flux times the pomeron structure function:

$$F_2^{D(4)}(Q^2, \beta, \xi, t) = f_{\mathbb{P}/p}(\xi, t) \cdot F_2^{\mathbb{P}}(Q^2, \beta) = \frac{K}{\xi^{1+2(\epsilon+\alpha't)}} F^2(t) \cdot F_2^{\mathbb{P}}(Q^2, \beta) \quad (12)$$

Since ξ is related to the rapidity gap, we will refer to this form of factorization as *gap factorization*. The parameter n of the ξ -dependence in (11) corresponds to the t -averaged value of $1 + 2(\epsilon + \alpha't)$ in (12), which we shall denote by n_{soft} to indicate its connection to the pomeron intercept obtained from soft collisions (total cross sections). With $\epsilon = 0.104$, $\alpha' = 0.25 \text{ GeV}^{-2}$, and $\langle |t| \rangle \approx 0.14 \text{ GeV}^2$ (for the ξ -range of the experiments), we obtain $n_{soft} = 1.14$. The values obtained by H1 and ZEUS are $n_{H1} = 1.19 \pm 0.06(stat) \pm 0.07(syst)$ and $n_{ZEUS} = 1.30 \pm 0.08(stat)_{-0.14}^{+0.08}(syst)$. Below, in a separate subsection, we will discuss the significance of the pomeron intercept measured at high Q^2 .

4.4 Breakdown of gap factorization

Rapidity gaps are expected to occur not only by the exchange of a pomeron, but also by the exchange of a meson. The Regge trajectories of the light mesons fall into three groups²:

$$\alpha_{f/a}(t) = 0.68 + 0.82t \quad \alpha_{\omega/\rho}(t) = 0.46 + 0.92t \quad \alpha_{\pi}(t) = 0 + 0.7t \quad (13)$$

Assuming that gap factorization holds for each exchange, $F_2^{D(4)}$ takes the form

$$F_2^{D(4)}(Q^2, \beta, \xi, t) = \sum_k f_{k/p}(\xi, t) \cdot F_2^k(Q^2, \beta) \quad (14)$$

where $k = \mathbb{P}$, f/a , ω/ρ or π , $f_{k/p}(\xi, t) \sim \xi^{1-2\alpha_k(t)}$ is the flux and $F_2^k(Q^2, \beta)$ the structure function of the particle represented by k . Interference terms between trajectories could also be added in (14). Gap factorization will break down if the pomeron F_2 structure is different than the meson structure. Motivated by (14), the H1 Collaboration fitted¹⁵ their 1994 data with the form

$$F_2^{D(3)}(Q^2, \beta, \xi) = F_2^{\mathbb{P}}(Q^2, \beta) \cdot \xi^{-n_{\mathbb{P}}} + C_M \cdot F_2^M(Q^2, \beta) \cdot \xi^{-n_M} \quad (15)$$

using as $F_2^M(Q^2, \beta)$ the GRV parametrization for the pion structure function and treating all other parameters as free. The fit yielded $n_{\mathbb{P}} = 1.29 \pm 0.03(stat) \pm 0.07(syst)$ and $n_M = 0.3 \pm 0.3(stat) \pm 0.6(syst)$. The trajectories calculated from these values, after accounting for the t -dependence, are $\alpha_{\mathbb{P}} = 1.18 \pm 0.02(stat) \pm 0.04(syst)$ and $\alpha_M = 0.6 \pm 0.1(stat) \pm 0.3(syst)$. The value of α_M is consistent with the value of $\alpha_{f/a}(0)$ in (13).

4.5 The pomeron intercept

There have been theoretical speculations, based on the Balitsky-Fadin-Kuraev-Lipatov (BFKL) QCD model of the pomeron¹⁶, that the effective pomeron intercept, $\alpha_{\mathbb{P}}(0)$, may increase with increasing Q^2 . The pomeron participating at high Q^2 interactions is generally referred to as “hard pomeron”, to distinguish it from the “soft pomeron” participating in soft processes. The question as to whether there exist two different pomerons is currently the subject of intense theoretical debate.

Experimentally, there is no conclusive evidence for two different pomerons, despite trends in the data that may advocate the contrary. Where signs of a “hard” pomeron appear in the data, usually other, more mundane, interpretations are possible. The pomeron intercept is a good example. Let us compare

Table 1: The pomeron intercept $\alpha_{\mathcal{P}}(0) = 1 + \epsilon$

| Measurement | Intercept |
|-------------------|--|
| Soft ² | 1.104 ± 0.002 |
| ZEUS-93 | $1.18 \pm 0.04_{-0.07}^{+0.04} = 1.18_{-0.08}^{+0.06}$ |
| H1-94 | $1.18 \pm 0.02 \pm 0.04 = 1.18 \pm 0.05$ |
| ZEUS-94 | $\epsilon_{hard} > \epsilon_{soft}$ (see text) |

the values of the intercepts measured at high Q^2 at HERA with the value of the soft pomeron intercept obtained from the total cross sections:

The HERA intercepts are systematically higher than the soft intercept, although statistically the effect is $\sim 1.5\sigma$. The question then is: do we really see the onset of the “hard” pomeron? Before answering this question, we comment on the ZEUS-94 measurement (last entry in Table 1). ZEUS measured the intercept from the cross section for $\gamma^*p \rightarrow Xp$ as a function of W^2 in the Q^2 range from 8 to 60 GeV². For a fixed diffractive mass, the cross section should vary as $(W^2)^{2\epsilon}$. In two data sets, one with $M_X < 3$ GeV and the other with $3 < M_X < 7.7$ GeV, the measured intercept values are in agreement with the H1 value, but show signs of a systematic increase with Q^2 within the limited statistics of the available data. Once again, is this a sign of the onset of the “hard” pomeron?

There are two important aspects of the ZEUS-94 data samples, which are evident from the relations $\beta \approx Q^2/(Q^2 + M_X^2)$ and $\xi \approx (Q^2 + M_X^2)/W^2$ obtained from (8):

- β is high, so that there is no substantial meson-exchange contribution.
- For fixed M_X^2 and Q^2 , $W^2 \sim \xi^{-1}$. Therefore, the W^2 -dependence of the cross section is, in effect, a ξ -dependence. Moreover, when M_X^2 is small and kept fixed, *regions of larger values of ξ are probed as Q^2 increases!*

Thus, what is perceived as an increase of the value of the intercept with Q^2 , is in fact a steepening of the ξ -distribution with increasing ξ . Such a steepening may be due to the de-coherence expected due to hadronic final state interactions, which should increase as the rapidity gap decreases.

The steepening of the ξ -distribution should be more prominent in the Tevatron high E_T diffractive dijet data, and in particular in the CDF “Roman Pot” data, for which $0.05 < \xi < 0.1$. Such an effect would reduce the dijet production rate at high ξ relative to that at small ξ .

In conclusion, the apparent increase of the pomeron intercept with Q^2 may be due to a gradual steepening of the ξ -distribution with increasing ξ

caused by a de-coherence effect due to final state interactions as the rapidity gap decreases. A measurement of the diffractive dijet rate as a function of ξ at the Tevatron can provide a decisive test of this hypothesis.

4.6 The structure of the pomeron

The shape (Q^2 and β dependence) of the pomeron structure function $F_2^{\mathbb{P}}(Q^2, \beta)$, presumed to be the term in $F_2^{D(3)}$ that contains the (Q^2, β) -dependence, was obtained by H1¹³ and ZEUS¹⁴ using fits of the form (11) on their 1993 data, and by H1¹⁵ using fit (15) on their 1994 data. All fits yielded an approximately flat β -distribution, within the measured range of $0.01 < \beta < 0.9$, and a Q^2 -distribution which, for $\beta < 0.65$, increases slowly (\sim logarithmically) by a factor of ~ 1.5 between $Q^2 = 10$ and $Q^2 = 60$ GeV². Above $\beta = 0.65$, the data (H1), which are all in a single β -bin centered at $\beta = 0.9$, show a flat Q^2 dependence. However, this β -bin includes a substantial contribution from vector mesons, whose relative magnitude decreases as Q^2 increases.

The gluon content of the pomeron was determined by ZEUS¹⁷ and H1¹⁵ using different techniques. ZEUS determined it by a combined analysis of the rate of diffractive DIS, which is mainly sensitive to the quark content of the pomeron, and the rate of diffractive inclusive jet production, $ep \rightarrow jet + X$ ($E_T^{jet} > 8$ GeV), which is sensitive to both the quark and gluon contents. This analysis yielded a hard-gluon fraction of $0.3 < f_g < 0.8$, *i.e.* 30% to 80% of the momentum of the pomeron carried by its partons is due to hard gluons. H1 derived the gluon content from the Q^2 -dependence of the $F_2^{D(3)}$ structure function. By interpreting this dependence as arising from scaling violations, and fitting the data using the DGLAP evolution equations, a QCD analysis led to the conclusion that gluons carry about 80% of the momentum of the pomeron at $Q^2 \sim Q_0^2 = 2.5$ GeV², and are concentrated at $\beta_{g/\mathbb{P}} = 1$. As Q^2 increases, the H1 analysis shows that the gluon content decreases slowly, while the quark content increases. However, these variations are very slow, so that at Q^2 values from ~ 25 to ~ 1000 GeV² the gluon fraction decreases from $\sim 80\%$ to $\sim 70\%$, and the quark fraction increases from $\sim 20\%$ to $\sim 30\%$, with both distributions remaining fairly hard (this conclusion is significant in using the H1 structure function of the pomeron to predict diffractive W and dijet production rates at the Tevatron).

Despite its appeal, the interpretation of the Q^2 -dependence of $F_2^{D(3)}$ as being due to scaling violations is not unique. Goulianos argued⁷ that the observed Q^2 -dependence is due to the pomeron flux renormalization, which we referred to earlier as *scaled gap probability*. A good fit to the data was obtained and, based on this fit, predictions for the rates of W and dijet production at the

Tevatron were made. As will be shown below, in the section “HERA versus Tevatron”, the renormalized/scaled flux predictions have now been confirmed by the CDF and DØ data.

5 Results from the Tevatron

Results on hard diffraction from the Tevatron have been reported by both the CDF and DØ Collaborations. One set of results was obtained using rapidity gaps as a tag for diffraction, while another by detecting the leading antiproton in a Roman Pot spectrometer. Figure 4 shows the event topology for dijet production in single diffraction, double diffraction and double pomeron exchange. Due to space limitations, double diffraction will not be discussed further.

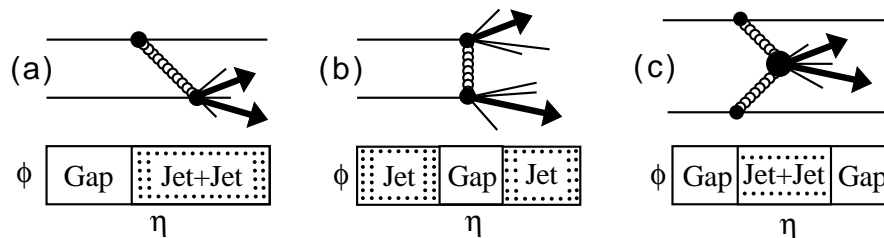


Figure 4: Dijet production diagrams and event topologies for (a) single diffraction (b) double diffraction and (c) double pomeron exchange.

Below, we will discuss first the rapidity gap results and then some Roman Pot results. All results are for $p\bar{p}$ collisions at 1.8 TeV unless otherwise stated. A confrontation between these results and predictions based on the diffractive structure function measured at HERA is planned for the next section.

5.1 Diffractive W production (CDF)

CDF made the first observation¹⁸ of diffractive W production and measured the production rate using a sample of 8246 events with an isolated central e^+ or e^- ($|\eta| < 1.1$) of $E_T > 20$ GeV and missing transverse energy $\cancel{E}_T > 20$ GeV. In searching for diffractive events, CDF studied the correlations of the Beam-Beam Counter (BBC) ($3.2|\eta| < 5.9$) multiplicity, N_{BBC} , with the sign of the electron- η , η_e , or the sign of its charge, C_e . In a diffractive $W^\pm \rightarrow e^\pm\nu$ event produced in a \bar{p} collision with a pomeron emitted by the proton, a rapidity gap is expected at positive η (p -direction), while the lepton is boosted towards negative η (angle-gap correlation). Also, since the pomeron is quark-flavor symmetric, and since, from energy considerations, mainly valence quarks from

the \bar{p} participate in producing the W , approximately twice as many electrons as positrons are expected (charge-gap correlation).

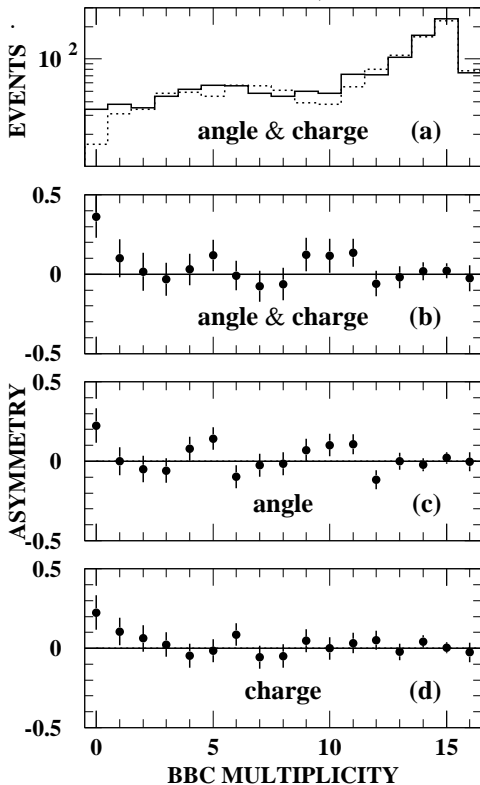


Figure 5: The diffractive W signal.

Figure 5 shows N_{BBC} distributions for two event samples, one with $\eta_e \eta_{BBC} < 0$ (angle-correlated) or $C_e \eta_{BBC} < 0$ (charge-correlated), and the other for $\eta_e \eta_{BBC} > 0$ (angle-anticorrelated) or $C_e \eta_{BBC} > 0$ (charge-anticorrelated). The *doubly-correlated* (anticorrelated, dotted) distributions, shown in Fig. 5a, are for events with $\eta_e C_e > 0$ and $\eta_e \eta_{BBC} < 0$ ($\eta_e \eta_{BBC} > 0$). Figure 5b shows the bin-by-bin asymmetry (difference divided by sum) of the two distributions of Fig. 5a. The excess seen in the first bin is the signature expected from diffractive events with a rapidity gap. An excess is also seen in the individual angle (Fig. 5c) and charge (Fig. 5d) asymmetries, as expected. The probability that the observed excess is caused by fluctuations in the non-diffractive background was estimated to be 1.1×10^{-4} .

Correcting for acceptance, the ratio of diffractive to non-diffractive W production is found to be:

$$R_W = [1.15 \pm 0.51(stat) \pm 0.20(syst)]\% \quad (\xi < 0.1)$$

The standard flux prediction for a two (three) flavor full hard-quark pomeron structure is $R_W^{hq} = 24\%$ (16%) and for a full hard-gluon structure $R_W^{hg} = 1.1\%$. The measured ratio favors a purely gluonic pomeron, but this is incompatible with the low fraction of diffractive $W + Jet$ events observed. A more complete comparison with theoretical predictions is made below in combination with the diffractive dijet CDF result.

5.2 Diffractive dijet production (CDF)

CDF searched for diffractive dijet production in a sample of 30352 dijet events with a single vertex (to exclude events from multiple interactions), in which the two leading jets have $E_T > 20$ GeV and are both at $|\eta| < 1.8$ or $|\eta| > 1.8$. No requirement was imposed on the presence or kinematics of extra jets in an event. Figure 6 shows the correlation of the BBC and forward ($|\eta| > 2.4$) calorimeter tower multiplicities in the η -region opposite the dijet system. The excess in the 0-0 bin is attributed to diffractive production. After subtracting the non-diffractive background and correcting for the single-vertex selection cut, for detector live-time acceptance and for the rapidity gap acceptance (0.70 ± 0.03), calculated using the POMPYT Monte Carlo program¹⁸ with pomeron $\xi < 0.1$, the ‘‘Gap-Jet-Jet’’ fraction (ratio of diffractive to non-diffractive dijet events) was found to be

$$R_{GJJ} = [0.75 \pm 0.05(stat) \pm 0.09(syst)]\% = (0.75 \pm 0.10)\% \\ (E_T^{jet} > 20 \text{ GeV}, |\eta|^{jet} > 1.8, \eta_1 \eta_2 > 0, \xi < 0.1)$$

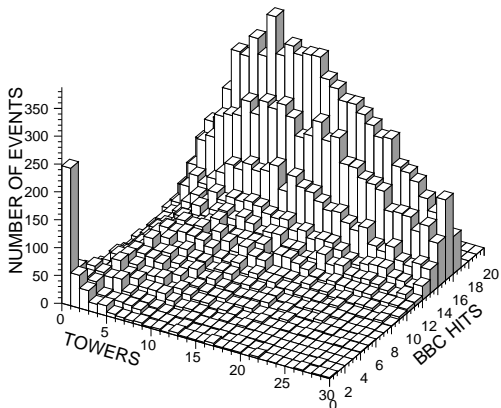


Figure 6: Tower versus BBC multiplicity for dijet events with both jets at $|\eta| > 1.8$ or $|\eta| < 1.8$.

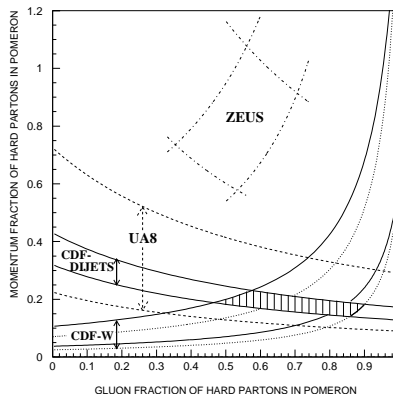


Figure 7: Total momentum fraction of partons in the pomeron versus gluon fraction.

5.3 The gluon fraction of the pomeron (CDF)

By combining the diffractive W and dijet results, CDF extracted the gluon fraction of the pomeron, f_g . Assuming the standard pomeron flux, the measured W and dijet fractions trace curves in the plane of D versus f_g , where D is the total momentum fraction carried by the quarks and gluons in the pomeron. Figure 7

shows the $\pm 1\sigma$ curves corresponding to the results. From the diamond-shaped overlap of the W and dijet curves, CDF obtain $f_g = 0.7 \pm 0.2$. This result, which is independent of the pomeron flux normalization, agrees with the result obtained by ZEUS¹⁷ from DIS and dijet photoproduction (dashed-dotted line in Fig. 7). For the D -fraction, CDF obtain the value $D = 0.18 \pm 0.04$. In the next section we will show that the decrease of the D -fraction at the Tevatron relative to that at HERA can be accounted for by the pomeron flux renormalization factor. The dashed lines are the $\pm 1\sigma$ curves for the UA8 diffractive dijet data. To compare UA8 with CDF, the UA8 fractions must first be multiplied by the ratio of the renormalization factors at the two energies, which is⁷ $D_{CDF}/D_{UA8} \approx 0.7$. Within the errors, the results of the two experiments are in good agreement.

5.4 Diffractive dijet production ($D\emptyset$)

$D\emptyset$ measured diffractive dijet production at $\sqrt{s} = 1800$ and 630 GeV using a rapidity gap tag. The $D\emptyset$ results, which are not corrected for acceptance, are shown in Fig. 8. The acceptance is expected to be of $\mathcal{O}(70\%)$. Thus, the $D\emptyset$ 1800 GeV fraction is in general agreement with the CDF measurement.

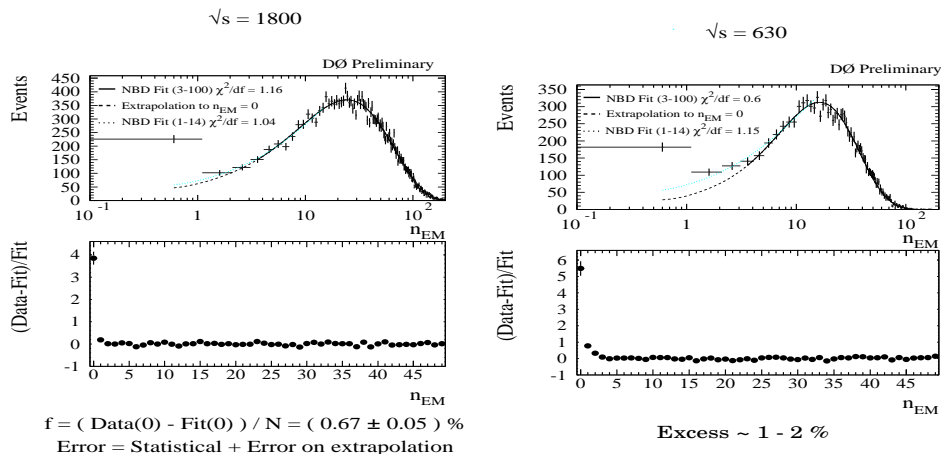


Figure 8: $D\emptyset$ results on diffractive dijet production:
(left) at $\sqrt{s} = 1800$ GeV and *(right)* at $\sqrt{s} = 630$ GeV.

The top figures show the calorimeter tower multiplicity in the forward region ($|\eta| > 2$) opposite the jets, and a fit to the data; the bottom figures show the ratio (data-fit)/fit. The excess in the first bin is the diffractive dijet signal.

5.5 Dijets in double-pomeron exchange

Both the CDF and the DØ Collaborations have observed dijet events produced by the interaction of two pomerons, one emitted by the p and the other by the \bar{p} . Using rapidity gaps at $|\eta| > 2$ to tag such events (see Fig. 4), DØ measured the ratio of double-pomeron exchange (DPE) to non-diffractive (ND) dijet events to be

$$\text{DØ result: } \sigma \left(\frac{\text{DPE}}{\text{ND}} \right)_{E_T^{j\text{et}} > 15 \text{ GeV}} = \mathcal{O}(10^{-6})$$

CDF tagged DPE dijet events by observing the leading antiproton in a Roman Pot spectrometer (Fig. 9) and a rapidity gap on the side of the proton.

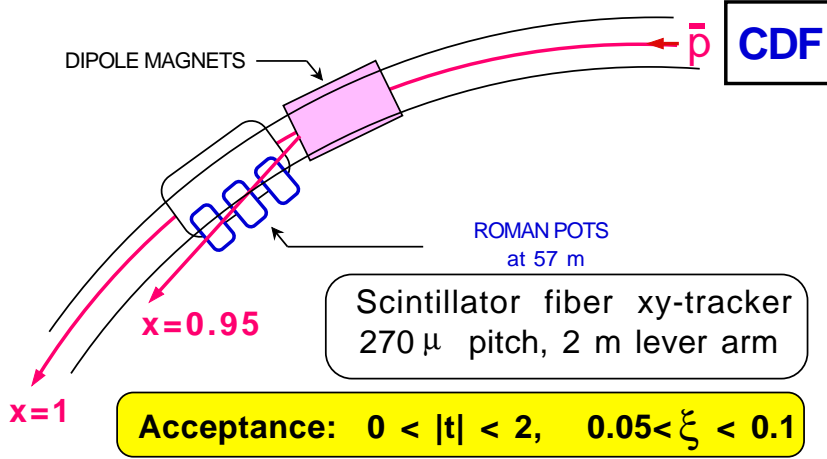


Figure 9: Schematic view of the CDF leading antiproton spectrometer

The \bar{p} trigger required the ξ of the pomeron from the \bar{p} to be within the range $0.05 < \xi_{\mathbb{P}/\bar{p}} < 0.1$, while from the rapidity interval covered by the BBC and from energy considerations it is estimated that the ξ of the pomeron on the p side lies approximately within the range $0.015 < \xi_{\mathbb{P}/p} < 0.035$. With these ξ -values, the energy in the $\mathbb{P} - \mathbb{P}$ center of mass system, $(\xi_{\mathbb{P}/\bar{p}} \cdot \xi_{\mathbb{P}/p} \cdot s)^{\frac{1}{2}}$, is approximately in the range 50-100 GeV. The DPE cross section was compared with the SD and non-diffractive (ND) dijet cross sections for $E_T^{j\text{et}} > 7$ GeV:

| | |
|------------------|---|
| DPE/SD | $[0.170 \pm 0.036(\text{stat}) \pm 0.024(\text{syst})]\%$ |
| SD/ND | $[0.160 \pm 0.002(\text{stat}) \pm 0.024(\text{syst})]\%$ |
| (DPE/SD)/(SD/ND) | 1.1 ± 0.3 |
| DPE/ND | $(2.7 \pm 0.7) \times 10^{-6}$ |

Assuming that both the p and \bar{p} pomeron fluxes are renormalized, the ratio enclosed in the box is expected to be ≈ 1 .

6 HERA versus Tevatron

The diffractive structure function measured in DIS at HERA can be used directly in PYTHIA to calculate the rate of diffractive W -boson production in $p\bar{p}$ collisions at the Tevatron. Such a calculation yields⁹ $R_W = 6.7\%$ for the ratio of diffractive to non-diffractive W production (a similar result has been obtained²⁰ by L. Alvero, J. Collins, J. Terron and J. Whitmore). The experimental value¹⁸ of $(1.15 \pm 0.55)\%$ is smaller than 6.7% by a factor of 0.17 ± 0.08 . The deviation of this factor from unity represents a breakdown of *QCD factorization*.

It has been shown⁹ that, assuming that the gap probability distribution in the DSF of (10) scales to the total gap probability, the ratio of the scaling factors between Tevatron and HERA is $D_{scale} = 0.19$. This factor agrees with the value of 0.17 ± 0.08 and with the momentum fraction of 0.18 ± 0.04 measured by CDF from the W and dijet rates. As mentioned earlier, the scaling of the gap probability is, in effect, the pomeron flux renormalization scheme proposed⁷ to unitarize the soft diffraction cross section. Thus, the breakdown of QCD factorization in hard diffraction is traced back to the breakdown of factorization in soft diffraction, which in itself is dictated by unitarity and is expressed as a scaling law of the gap probability distribution.

7 Conclusion

Experiments at HERA and at $p\bar{p}$ Colliders show that the pomeron has a hard partonic structure, which is dominated by gluons but has a substantial quark component. The DSF of the proton, measured in DIS at HERA, fails to predict the diffractive W and dijet rates measured at the Tevatron. This breakdown of factorization is restored by scaling the rapidity gap probability distribution, which appears as a factor in the DSF, to the total gap probability. The scaling of the gap probability is also needed to explain the s -dependence of the soft $p\bar{p}$ SD cross section. Assuming that the gap is caused by pomeron exchange, no breakdown of factorization occurs in the hard collision between the pomeron and the γ^* at HERA or between the pomeron and the $p(\bar{p})$ at the Tevatron.

Two questions that have been raised are: (a) Is the Q^2 dependence of the DSF due to QCD scaling violations or due to the scaling of the gap probability? (b) Does the apparent increase of the pomeron intercept with Q^2 come from an increase with pomeron- ξ due to hadronic final state interactions?

References

1. K. Goulianos, Physics Reports **101** (1983) 169.
2. R.J.M. Covolan, J. Montanha and K. Goulianos, Phys. Lett. **B 389** (1996) 176.
3. G. Ingelman and P. Schlein, Phys. Lett. **B 152** (1985) 256.
4. P. Bruni and G. Ingelman, Preprint DESY-93-187; Proceedings of the International Europhysics Conference on High Energy Physics, Marseille, France, 22-28 July 1993, Editions Frontières (Eds. J. Carr and M. Perrottet) p.595.
5. T. Sjöstrand, Comput. Phys. Comm. **82**, 74 (1994).
6. A. Donnachie and P. V. Landshoff, Nucl. Phys. **B 303** (1998) 634.
7. K. Goulianos, Phys. Lett. **B 358** (1995) 379; *ib.* **B363** (1995) 268.
8. K. Goulianos, Proceedings of the 3rd Workshop on Small-x and Diffractive Physics, Argonne National Laboratory, USA, 26-29 September 1996.
9. K. Goulianos, Proceedings of the 5th International Workshop on Deep Inelastic Scattering and QCD (DIS-97), Chicago, USA, 14-18 April 1997.
10. K. Goulianos, Proceedings of the 10th Topical Workshop on Proton-Antiproton Collider Physics, Fermilab, Batavia, IL, USA, 9-13 May 1995.
11. A. Brandt et al. (UA8 Collaboration), Phys. Lett. **B297** (1992) 417; R. Bonino *et al.* (UA8 Collaboration), Phys. Lett. **B211** (1988) 239.
12. P. Schlein, *Evidence for Partonic Behavior of the Pomeron*, Proceedings of the International Europhysics Conference on High Energy Physics, Marseille, France, 22-28 July 1993 (Editions Frontières, Eds. J. Carr and M. Perrottet).
13. T. Ahmed *et al.*, Phys. Lett. **B 348** (1995) 681.
14. M. Derrick *et al.*, Z. Phys. **C68** (1995) 569
15. H1 Collaboration: *A Measurement and QCD Analysis of the Diffractive Structure Function $F_2^{D(3)}$* , Contribution to ICHEP'96, Warsaw, Poland, July 1996.
16. L. N. Lipatov, Sov. J. Nucl. Phys. **23**, 338 (1976); E. A. Kuraev, L. N. Lipatov and V. S. Fadin, Sov. Phys. JETP **44**, 443 (1976); Sov. Phys. JETP **45**, 199 (1977); Ya. Ya. Balitsky and L. N. Lipatov, Sov. J. Nucl. Phys. **28**, 822 (1978).
17. M. Derrick *et al.*, Phys. Lett. **B 356** (1995) 129.
18. F. Abe *et al.*, Phys. Rev. Lett. **78** (1997) 2698.
19. F. Abe *et al.*, "Measurement of Diffractive Dijet Production at the Fermilab Tevatron", submitted to Phys. Rev. Letters.
20. J. Whitmore, Proceedings of the 5th International Workshop on Deep Inelastic Scattering and QCD (DIS-97), Chicago, USA, 14-18 April 1997.